pp 1898–1918. © Royal Aeronautical Society 2019
doi:10.1017/aer.2019.12

Effects of chemical reaction mechanism and NO_x formation pathways on an inter-turbine burner

A. A. V. Perpignan and A. Gangoli Rao
A.GangoliRao@tudelft.nl
Faculty of Aerospace Engineering
Delft University of Technology
Delft, the Netherlands

ABSTRACT

One of the main challenges of future aircraft engines is to achieve low pollutant emissions while maintaining high combustion efficiencies and operability. The Flameless Combustion (FC) regime is pointed as one of the promising solutions due to its well-distributed reaction zones that yield low NO_x emissions and oscillations. A dual-combustor configuration potentially facilitates the attainment of FC in the Inter-Turbine Burner (ITB). The development of such burner is dependent on knowledge regarding NO_x formation and the parameters affecting it. It is known from the literature that the NO_x formation mechanisms are different in FC. Therefore, in an attempt to clarify some of the mechanisms involved in NO_x formation at relevant conditions, a chemical reactor network model developed to represent the ITB is explored. The role of prompt NO_x was previously shown to be dominant at relatively low inlet temperatures and atmospheric pressure. In order to check these findings, five chemical reaction mechanisms were employed. All of them overpredicted NO_x emissions and the overprediction is likely to be caused by the prompt NO_x subset implemented in these mechanisms. Higher reactants temperatures and operational pressures were also investigated. Overall NO_x emissions increased with temperature and the NO_x peak moved to lower equivalence ratios. Operational pressure changed the emissions trend with global equivalence ratio. Leaner conditions had behaviour similar to that of conventional combustors (increase in NO_x), while NO_x dropped with further increase in equivalence ratio due to suppression of the prompt NO_x production, as well as an increase in NO reburning. These trends highlight the differences between the emission behaviour of the ITB with those of a conventional combustion system.

Keywords: Flameless combustion; Gas turbine combustion; MILD combustion; NO_x chemistry

Received 1 October 2018; revised 21 December 2018; accepted 25 February 2019.
A version of this paper was presented at the 24th ISABE Conference in Canberra, Australia, September 2019.

NOMENCLATURE

Abbreviation

CFD	Computational Fluid Dynamics
CRN	Chemical Reactor Network
FC	Flameless Combustion
ITB	Inter-Turbine Burner
PaSR	Partially Stirred Reactor
PSR	Perfectly Stirred Reactor

Symbol

p	Pressure
RR	Recirculation Ratio
T	Temperature
Φ	Global equivalence ratio

Subscripts

in	Reactants

1.0 INTRODUCTION

The contribution of aviation to the emission of pollutants and greenhouse gases is estimated to increase despite the urgency for reducing emissions. Emissions of CO_2 by international aviation were projected to increase by 144% between 2005 and 2025[1] and the increase in CO_2 emissions in China is projected to be 3.9% per year from 2013 till 2030[2]. Subsequent to the required reduction in CO_2 emissions, emission of minor pollutants such as CO and nitrogen oxides (NO_x) also require attention. The photochemical smog and acid rains are caused by NO_x, while NO_2 is a greenhouse gas formed by the oxidation of NO in the atmosphere[3]. Moreover, non-CO_2 pollutants behave differently when emitted at high altitude. For example, NO_x contribute to the formation of O_3 in the troposphere, a greenhouse gas[4].

This scenario clearly suggests that innovation is required to keep up with the market growth while attaining the required reductions in emissions. Innovation is possible at many levels, from comprehensive solutions such as new aircraft configurations and alternative energy sources, to substantial improvements in combustion technology. Given the challenging nature of these goals, it is likely that the solution has to involve all levels.

The Flameless Combustion (FC) regime (also known as MILD combustion) has been pointed as a promising combustion technology, as it has the potential to maintain high combustion efficiency while achieving lower NO_x emissions. The regime takes place at relatively high reactants' temperatures and low O_2 concentrations and is characterized by highly distributed reaction zones that yield lower peak temperatures and NO_x emissions[5]. While FC is successfully applied to industrial furnaces, the challenges pertaining to the attainment of the FC regime in gas turbines were summarized by Perpignan et al.[5] as: high power/heat density, low overall equivalence ratio, heat transfer characteristics, wide operating envelop and pressure loss requirements.

Conceptual design attempts for FC combustors relied on the recirculation of combustion products, either jet induced or by having large recirculation zones formed due to their

https://doi.org/10.1017/aer.2019.12 Published online by Cambridge University Press

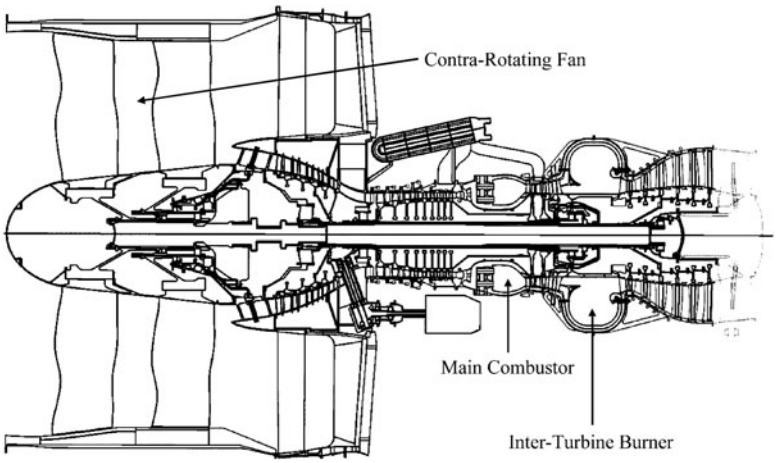

Figure 1. Engine concept with an inter-turbine burner. Courtesy of Pratt and Whitney Rzeszów S.A., Copyright 2014.

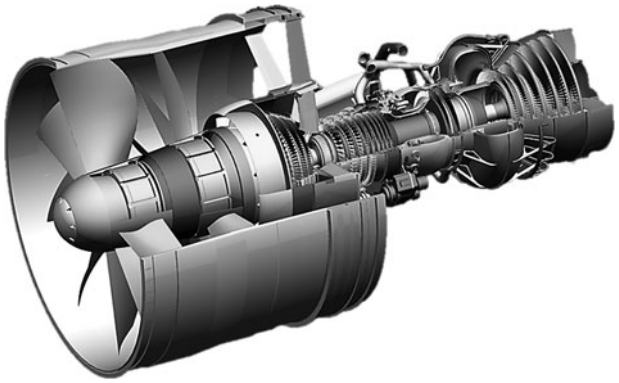

Figure 2. The hybrid dual-combustor engine. Courtesy of Pratt and Whitney Rzeszów S.A., Copyright 2014.

geometries. However, the resulting operational ranges were usually narrow. Moreover, emissions posed problems, as CO tended to increase when NO_x was at desirable levels and vice versa. Proposing a more comprehensive solution, the Advanced Hybrid Engines for Aircraft Development (AHEAD) project[6] involved the use of two sequential combustion chambers, having the high-pressure turbine between them (see Fig. 1).

The hybrid engine was designed to operate using fuels stored cryogenically in the first combustor and conventional or biofuels in the Inter-Turbine Burner (ITB). Additionally, the concept takes advantage of the presence of cryogenic fuels to cool the bleed air prior to its utilization to cool turbine vanes and blades, reducing the required air mass flows and, therefore, reducing losses. This process is also beneficial due to the preheating of the fuels prior to their entry in the main combustor. Another feature of the engine is the use of a contra-rotating fan, as shown in Fig. 2. As the aircraft was conceptualized as a blended wing body and the engines are positioned at the aft of the fuselage to allow for boundary layer ingestion, the contra-rotating configuration is advantageous because it enables more compact fans and

https://doi.org/10.1017/aer.2019.12 Published online by Cambridge University Press

higher propulsive efficiency at a given bypass ratio[7]. From a combustion point of view, the configuration with two combustors facilitates the attainment of the FC regime in the second combustor, the ITB. This proposed inter-turbine flameless combustor is studied in the present paper.

Even though the concept looks promising[8], it has to be further developed as there are many unknowns. The design of an ITB, or any other combustor intending to employ FC, relies on accurate prediction and representation of both fluid dynamics and chemistry. Chemical kinetics is particularly important for the prediction of pollutant emissions since low emissions are the goal of employing FC in the first place.

1.1 Chemical kinetics under the FC regime

Even though there is not yet a consensus on the definition of FC, its beneficial characteristics are well documented. The well-distributed fashion in which reactions take place tends to cause low temperature gradients, low NO_x emissions, stable reaction zones and low acoustic oscillations[9]. The lower NO_x emissions are caused by the more homogeneous reaction zones that abate thermal NO_x; by the reduction in the availability of the species involved in NO_x formation, especially O_2; and due to the effect on the production of NO_x through the NNH, N_2O-intermediate and prompt formation pathways[5]. However, the ways in which the pathways are influenced under FC and what parameters govern such influence are not yet fully understood.

The use of ideal chemical reactors to model the chemical processes in FC is a powerful tool because it allows the use of detailed chemical reaction mechanisms at relatively low computational costs. Additionally, the assumptions and simplifications of such reactors usually fit well with the distributed reactions conditions linked to FC. Nicolle and Dagaut[10] showed interesting results by using partially stirred reactor calculations. The authors pointed to the contribution of the N_2O pathway to be as important as that of thermal NO_x, as well as the relevant contribution of both NNH and prompt pathways. The occurrence of NO reburning was also relevant. The high recirculation usually present in FC systems increases NO reburning. Since the first studies on FC[11], different chemical mechanisms to take reburning into account have been proposed[12,13].

For conventional gas turbine combustors, the thermal (or Zel'dovich) pathway is constantly pointed as the dominant source, with minor contributions of prompt and N_2O-intermediate pathways, the latter for leaner conditions[14,15]. The conditions for increased N_2O impact were already associated with more distributed conditions (before any mention to FC), as described by Correa[14]. However, the formation (and destruction) of NO_x can occur through more pathways, as recently reviewed by Glarborg et al.[3], as the authors added the NNH pathway, NO reburning, as well as the oxidation mechanisms of HCN, HNCO and NH_3 (as fuel-NO_x subsets), to the thermal, prompt and N_2O pathways.

It has been shown that NO_x emissions may display a non-monotonic behaviour with increasing equivalence ratio, with the peak being at lean equivalence ratios in systems in which the FC regime is attained via high recirculation of combustion products. It is known that NO_x emissions usually peak on the lean side with changing equivalence ratio, but just adjacent to stoichiometry[16], as the competition between fuel and nitrogen for O_2 to oxidize reduces NO_x at stoichiometry. The behaviour shown for some FC applications is, however, at values further away from stoichiometry, as shown in Fig. 3.

https://doi.org/10.1017/aer.2019.12 Published online by Cambridge University Press

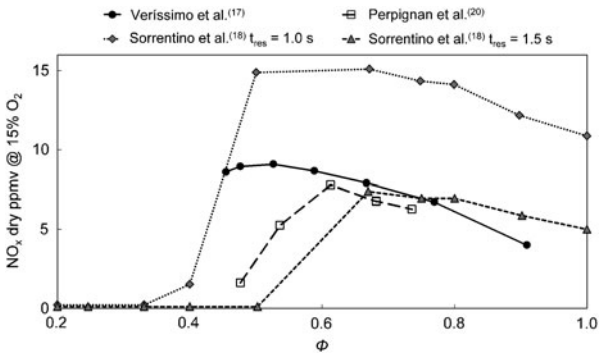

Figure 3. Measured NO_x emissions as a function of equivalence ratio for three different systems with high recirculation: a combustion chamber with jet-induced stabilization[17], an inter-turbine burner[20], and a cyclonic prismatic chamber for two different estimated residence times[18]. The values from Perpignan et al.[20] are shown with respect to the local equivalence ratio, and not the global equivalence ratio, as defined by the authors.

The three systems depicted in Fig. 3 have significant differences between each other. The work of Veríssimo et al.[17] utilized a cylindrical combustion chamber with a jet-based burner, in which the central air jet was surrounded by 16 CH_4 jets. The prismatic combustion chamber utilized by Sorrentino et al.[18] is characterized by a large central recirculation zone and relatively high residence times. Air and C_3H_8 were added to the chamber via pipes positioned in two opposing corners of the chamber. Lastly, the model combustor based on the design presented by Levy et al.[19] (an 18-degree sector aimed at representing the ITB) had some of its experimental data presented by Perpignan et al.[20]. It was fuelled by CH_4 and the inlet oxidiser could be pure or diluted air. Despite being different, all combustors were aimed at attaining FC and showed a similar NO_x emissions behaviour with respect to equivalence ratio.

The authors, however, provided different explanations for this behaviour in each case. Veríssimo et al.[17] pointed to a switch between FC and conventional lean combustion caused by mixing characteristics between the burner jets and the recirculating combustion products. Sorrentino et al.[18] explained that higher temperatures were attained at the prismatic combustion chamber at higher equivalence ratios, which activated NO reburning. Lastly, supported by results from a chemical reactor network (CRN), Perpignan et al.[20] showed the prominent role of prompt NO_x formation in the non-monotonic behaviour.

The use and development of CRNs have been done both in manual[21–23] and automated forms[24–26]. Both approaches have shown good results with respect to predicting emissions. The development of CRNs requires a degree of knowledge about the flow field in order to divide the domain into areas of similar expected conditions (temperature, concentrations, velocity, and/or fluctuations). This preceding knowledge may come from CFD simulations or experiments.

The present work intends to further investigate the effects of recirculating combustion products, to compare the performance of chemical reaction mechanisms for CH_4combustion, and to understand the effect of T and p on the NO_x emissions of the ITB. This is performed by utilizing CRNs and the modelling approach described in Section 2.

https://doi.org/10.1017/aer.2019.12 Published online by Cambridge University Press

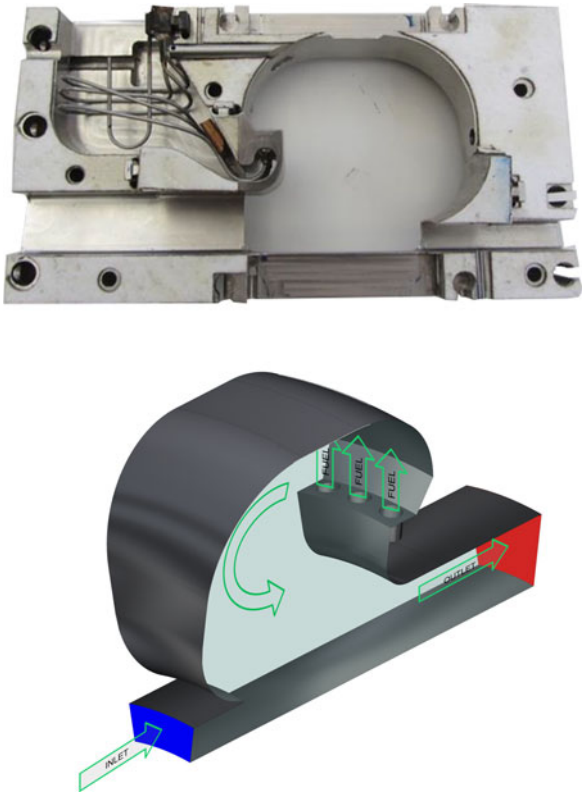

Figure 4. Schematic of the model combustor employ for experiments[18]. The 18-degree sector contained three fuel ports, which were fed along with oxidizer. The remainder of the oxidizer was fed through the port indicated in blue. The side walls were quartz windows to allow visualisation.

1.2 The ITB experimental model

The ITB and the CRN developed to represent its experimental model are the focus of the present paper. The 18-degree sector model was developed to mimic the phenomena expected on the full-scale ITB designed by Levy et al.[19] and had three CH_4 injectors that entered the chamber along with a coflow of oxidizer (combustion air). Another portion of the oxidizer (dilution air) entered the chamber via a different port (see Fig. 4). Reactions took place in the large recirculation zone. The oxidizer was preheated to 560 K and the experiments were performed at atmospheric pressure.

The analysis performed by Perpignan et al.[20] showed that the developed CRN was able to reproduce the experimental results to a good extent and there were significant differences between the two chemical reaction mechanisms employed (GRI 2.11 and GRI 3.0). The reasons for such differences were not entirely clear, although there was evidence that the prompt NO chemistry was responsible.

The development of the ITB concept, and of FC in general, is highly dependent on the computational tools' ability to accurately predict pollutant emissions since the design is aimed at taking advantage of the vitiated oxidiser to reduce emissions. Therefore, assessing and understanding the performance of chemical reaction mechanisms is of great importance. Moreover, the understanding regarding the NO_x emissions in systems with high recirculation intended to operate under the FC regime is still limited.

https://doi.org/10.1017/aer.2019.12 Published online by Cambridge University Press

2.0 NUMERICAL SIMULATIONS

In order to understand the effects of recirculating combustion products on NO_x emissions, as well as the effects of different chemical reaction mechanism and operating conditions, numerical simulations were carried out. The CRN simulations were comprised of two different approaches. Firstly, a simple CRN was developed to systematically evaluate the effect of recirculation, equivalence ratio and residence times on NO_x emissions behaviour. Secondly, the CRN of the ITB (developed by Perpignan et al.[20]) was used to evaluate the chemical reaction mechanisms and operating conditions relevant for the ITB application and development. All simulations were performed using Cantera[27], an open-source computational tool focused on chemical kinetics.

The CRN approach allows the use of detailed chemical reaction mechanisms. The current work explored five different mechanisms for CH_4 combustion: GRI 2.11[28], GRI 3.0[29], Konnov[30], GDF-Kin® 3.0 NCN[31] and POLIMI C1C3HT[32].

The Gas Research Institute (GRI) mechanisms[28,29] were developed with an aim of representing methane and natural gas flames and their ignition. The GRI 2.11 is comprised of 49 species and 277 reactions. The GRI 3.0 comprises 53 species and 325 reactions and has been optimized for conditions between 1,000 and 2,500 K, $1.333 \cdot 10^3$ to $1 \cdot 013 \cdot 10^6$ Pa, and equivalence ratios from 0.1 to 5 in premixed systems.

The Konnov mechanism[30] was developed to model the combustion of H_2, CO, CH_2O, CH_3OH, CH_4 and C2-C3 hydrocarbons[33]. The mechanism comprises 129 species and 1,231 reactions. The original mechanism underwent modifications related to the prompt NO pathway: instead of the HCN route, the NCN route was implemented. The same route is present in the GDF-Kin® 3.0 NCN mechanism[31], as the authors compared the performance of the mechanism with both routes. Intended to simulate natural gas combustion, the mechanism is composed of 119 species and 883 reactions.

Lastly, the POLIMI C1C3HT[32] was developed to simulate the combustion and pyrolysis of hydrocarbons with up to 3 carbon atoms. Its development was mostly based on flame speed data for several species (H_2 and H_2/CO mixtures, small and large hydrocarbons, alcohols and hydrocarbon mixtures). The prompt NO_x HCN route is adopted in the mechanism. The mechanism contains 115 species and 2,141 reactions.

In order to quantify the contributions of each formation pathway, the CRN was also run with deactivated reactions. The deactivated reactions for each pathway in each chemical reaction mechanism are shown in the Appendix.

2.1 Four-reactor CRN

As discussed in Section 1.1, the recirculation of combustion products employed to attain the FC regime is one of the main factors involved in the reduction of NO_x. However, its effects are not fully understood, and to elaborate on the involved phenomena, a simple CRN composed of four PSRs was developed to showcase the effect of recirculation and equivalence ratio on NO_x emissions (Fig. 5). Moreover, the simple model enables the discussion of some of the results attained with the ITB model. The names of the PSRs in Fig. 5 are merely representative of the expected function each PSR is expected to have in the simulations. The combustor PSR was assigned with 75% of the total volume, while the mixer, outlet and recirculation PSRs had 15, 6 and 4%, respectively. Different total volumes were assigned in order to assess the effect of residence time. Heat losses were included since they are present in virtually every experimental investigation related to FC (including the works from Fig. 3). Losses play an important role in NO_x formation under FC, especially due to

https://doi.org/10.1017/aer.2019.12 Published online by Cambridge University Press

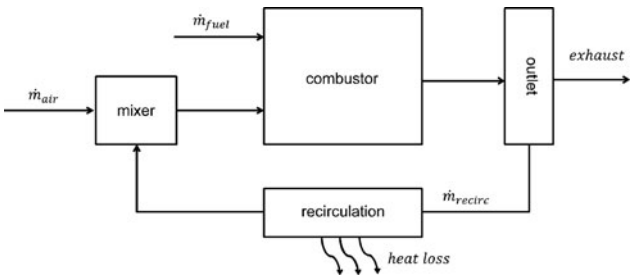

Figure 5. Scheme of the CRN designed to investigate the effect of recirculation of products in the behaviour of NO_x emissions

their effect on the thermal pathway. All simulations of this CRN were performed using the GRI 3.0 mechanism.

Different values of Φ were tested. The total amount of mass flow was kept constant, causing both air and fuel mass flows to be different for each value of Φ. The amount of recirculation was quantified by the recirculation ratio (*RR*), shown in Equation (1)

$$RR = \frac{\dot{m}_{recirc}}{\dot{m}_{air} + \dot{m}_{fuel}} \tag{1}$$

2.2 Four-reactor CRN results and limitations

The four-reactor CRN results are shown first in order to discuss some general aspects of systems with high recirculation and the difficulties in modelling emissions in such systems. Examining the effect of recirculation, an increase in *RR* for the same value of T_{in} and Φ may increase or decrease NO_x. Additionally, the influence of *RR* on the absolute values of NO_x is quite low for the settings used in Fig. 6. The differences caused by *RR* are less than 1 ppm.

Nevertheless, analysing the results in Fig. 6, it is possible to notice that recirculation of products has two competing effects: on one hand, the composition of the products tends to reduce reaction rates of the incoming reactants; on the other hand, the products have high temperatures, which tends to increase reaction rates. This explains why for leaner cases, higher *RR* tends to increase NO_x, as combustion products contain larger amounts of O_2 and N_2 available for the oxidation.

The sub-ppm changes in NO_x emissions with changing *RR* in this CRN model can be explained by the large relative size of the combustor reactor and the very assumption underlying a PSR, namely perfect and instantaneous mixing. The large volume of the reactor causes most of the reactions to take place in that reactor. Therefore, the temperature rise occurs in it and adding combustion products has little influence in heating up the incoming reactants.

In a simple model as the present CRN, residence times play an even more central role. The simulations were performed maintaining the total mass flow constant. However, as the temperature increase is lower for leaner cases, these had higher residence times due to lower density. The plot in Fig. 7 shows how the NO_x emissions behave with Φ for three different volume settings. For residence times varying from 0.49 to 0.76 s across the values of Φ (case 1 in Fig. 7), lower Φ causes higher NO_x. On the other hand, when the values vary from 0.103 to 0.171 s (case 3 in Fig. 7), NO_x increases with Φ. This is explained by two effects: (i) the increasing NO_x due to longer time available for reactions to proceed and (ii) the increasing

https://doi.org/10.1017/aer.2019.12 Published online by Cambridge University Press

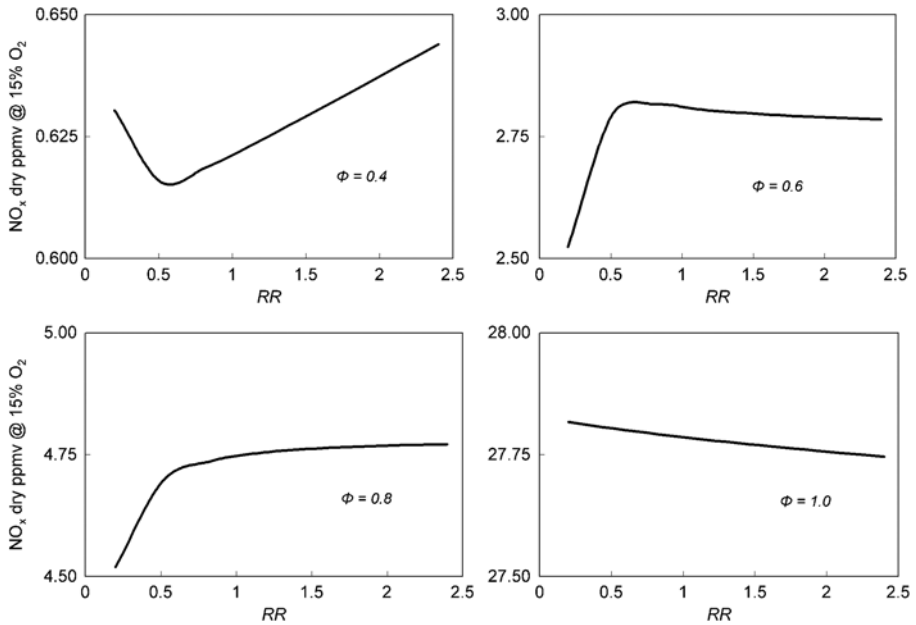

Figure 6. NO_x emissions as a function of RR for the four-reactor CRN. Four different Φ. Mean residence time = 0.12 s. T_{in} = 600 K.

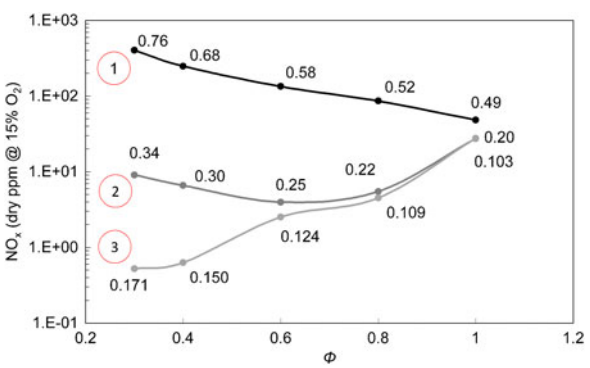

Figure 7. NO_x emissions as a function of Φ for the four-reactor CRN. Three different reactor volume settings. Values of residence time shown in seconds for each data-point. T_{in} = 600 K. RR = 0.2.

NO_x due to reactants being exposed to higher temperatures. The case varying from 0.20 to 0.34 s (case 2) has a non-monotonic trend, indicating the shift between these two effects.

The overall NO_x behaviour is complex and is dependent on the temperatures attained in the reactors, residence time, and recirculation ratio. Understanding the complexity and how the parameters involved act aids the analysis of the ITB CRN.

2.3 The inter-turbine burner CRN

The CRN employed for the ITB simulations was developed and employed by Perpignan et al.[20]. The regions assigned to each reactor were based on the results of CFD calculations,

https://doi.org/10.1017/aer.2019.12 Published online by Cambridge University Press

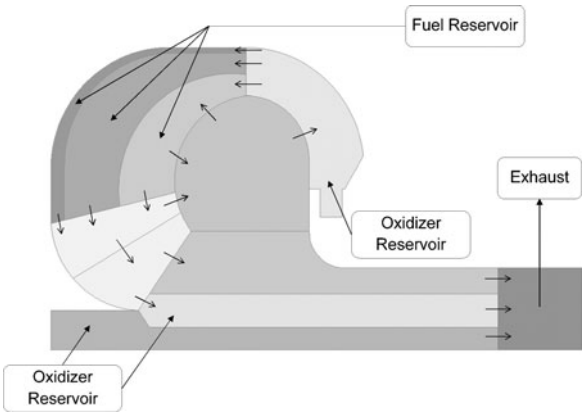

Figure 8. The CRN developed by Perpignan et al.[20]. Each region of the combustor was represented by a PSR. Arrows indicate the presence of mass exchange between reactors or reservoirs.

like velocity, temperature and species concentrations fields, were taken into account to divide the domain. The resulting CRN had 11 PSRs, as shown in Fig. 8.

The recirculation inside the ITB was one of the most important factors to reproduce experimental data. The mass flows between the reactors were estimated based on the CFD simulations. Heat losses were assigned to each reactor based on the available temperature measurements and on the temperature attained inside the reactor.

3.0 RESULTS AND DISCUSSION

The results regarding the ITB are discussed in this section. A comparison between the different chemical reaction mechanisms is drawn in Section 3.1. The subsequent sections discuss the results of different reactants temperature (Section 3.2) and operating pressure (Section 3.3).

3.1 Chemical reaction mechanisms

Comparing the various available chemical reaction mechanisms is important in order to understand as to how they differ in their performance and to check the dependency of the resulting emission trend on the mechanism. The results of Fig. 9 show that all mechanisms are able to predict the non-monotonic trend while overpredicting the emissions of the ITB. The reason for the overprediction appears to be the prompt NO_x formation, which plays an important role according to all chemical reaction mechanisms. Apparently, the results are independent of the NCN pathway for prompt formation (instead of HCN), as it is nowadays known to be the way reactions proceed[3]. The POLIMI and both GRI mechanisms (2.11 and 3.0) consider prompt NO_x via the HCN route, while the other two mechanisms employ the NCN route.

Previous studies have shown that the relative importance of the NNH and N_2O-intermediate pathways increases under FC[34]. However, the contribution of prompt NO_x is responsible for the difference between the mechanisms in this case. Table 1 shows that the overprediction shown in Fig. 9 is correlated with the mean contribution of prompt NO_x.

The results suggest that there is a systematic overprediction of prompt NO_x. It is unclear whether this is universal for every system with recirculation of combustion products.

https://doi.org/10.1017/aer.2019.12 Published online by Cambridge University Press

Table 1
Results for the different chemical reaction mechanisms across the investigated equivalence ratios with respect to prompt NO_x contribution and deviation from experiments

Mechanism	Prompt NO_x Mean Contribution	Mean Deviation from Experiments
GRI 2.11	43.1%	1.93
Konnov	45.5%	2.98
GRI 3.0	67.7%	4.71
POLIMI C1C3HT	76.3%	4.76
GDF-Kin® 3.0 NCN	85.0%	7.30

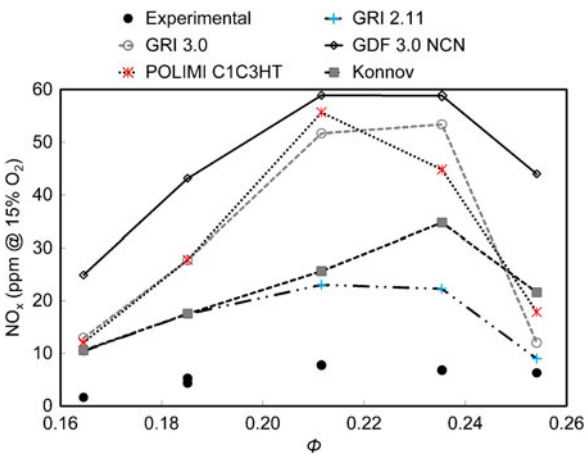

Figure 9. NO_x emissions as a function of global equivalence ratio for various chemical reaction mechanisms.

However, further studies should be focused on prompt NO_x chemistry in order to clarify if reaction rates should be lower when vitiated conditions are attained, or if reactions progress through different routes.

3.2 Effect of reactants temperature on the ITB

The investigation for higher temperatures and pressures was conducted using the GRI 2.11 mechanism, due to its better performance when compared to experiments. These conditions were investigated to achieve settings closer to those expected in the dual-combustor engine[6].

Increasing temperatures cause the overall contribution of prompt NO_x to decrease, as thermal NO_x tends to increase its contribution (Fig. 10). Moreover, the role of prompt NO_x in causing the non-monotonic behaviour is no longer important for higher inlet temperatures. Instead, the NNH pathway becomes the most important driver.

The overall trend of NO_x emissions is maintained with increasing temperatures. However, the higher the T_{in}, the leaner is the NO_x peak located. This is partially explained by the effect

https://doi.org/10.1017/aer.2019.12 Published online by Cambridge University Press

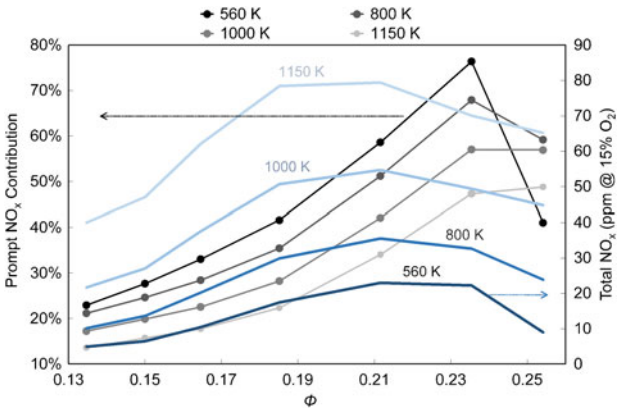

Figure 10. Total NO_x emissions and relative prompt NO_x contribution as functions of global equivalence ratio for various T_{in}.

of residence time, in a similar fashion of that shown in Section 2.2. As the power input is maintained for every case, higher T_{in} causes lower residence times due to the decrease in density. This shows that the volume of the ITB (for a given design) can be optimized for a given inlet temperature. In turn, T_{in} is determined by the power setting, the energy fraction between the main combustor and the ITB and the high-pressure turbine pressure ratio.

3.3 Effect of operating pressure on the ITB

For conventional combustors, the scaling of NO_x has been reported to follow the expression of Equation (2). The exponent n usually has a value between 0.5 and 0.8 for values closer to stoichiometry[15], while leaner equivalence ratios are not usually affected by p, having n equal to 0[14]. For the comparison carried out in Fig. 11, the value of n was assumed to be 0 at the leanest condition and it was increased linearly up to 0.65 for the richest case.

$$\boldsymbol{NO_x = (p^n)\ NO_x @\ 1\ atm} \tag{2}$$

The effect of pressure on NO_x emissions is more complex than that of temperature, as shown in Fig. 11. The leaner portion of the investigated Φ behaves similarly to conventional combustors: higher pressures increase NO_x emissions as in Equation (2). The increase is caused by the increase in residence times at higher p, similarly to the effect described in Section 2.2. At $\Phi \approx 0.21$, NO_x emissions drop below the value attained at 1 bar.

Perpignan et al.[20] showed that at this point, thermal NO_x starts decreasing (for $p = 1$ bar) while reburning and prompt increase, with the former becoming dominant along with the NNH pathway. The reduction of the thermal pathway (caused by the favourable conditions for reburning) and the increase in reburning still occurs for higher p. However, the prompt NO_x contribution is lower, a known effect of increasing p[14,35]. Additionally, the NNH pathway has lower production than at $p = 1$ bar. Subsequently, NO_x emissions increase at the richer condition due to an increase in the thermal and N_2O-intermediate pathways, indicating that the higher temperatures attained at higher Φ play a more important role for the overall NO_x formation.

https://doi.org/10.1017/aer.2019.12 Published online by Cambridge University Press

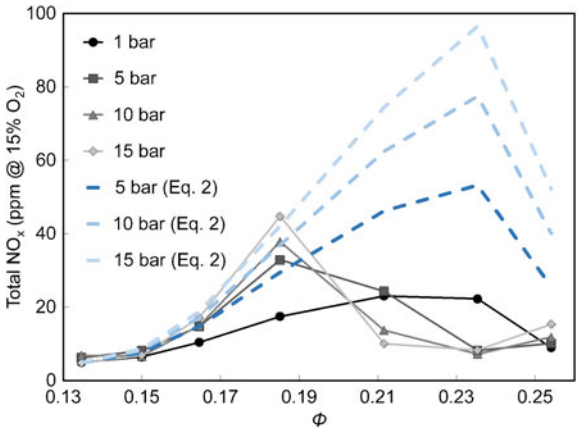

Figure 11. NO_x emissions as a function of global equivalence ratio for various operational pressure values of the ITB CRN. Dashed lines represent the values obtained when considering the correlation of Equation (2).

The results suggest that experimental data on emissions at high pressures for systems intended to operate under the FC are necessary. Given the reported importance of prompt NO_x as a contributor at atmospheric pressures, the design of an ITB may take advantage of its suppression at higher pressures.

3.4 Overall comments

The non-monotonic NO_x emission curves with lean Φ shown in Fig. 3 were explained differently by their authors. Given the complexity of the phenomena involved, as shown in the current analysis, it may be the case that the results are truly caused by different reasons.

In view of the influence of residence time shown in Fig. 7, the results of Sorrentino et al.[18] may be a consequence of a similar phenomenon. As temperatures were higher for higher Φ, residence times tended to be lower due to the reduction in density, justifying the lower NO_x emissions. This effect is not likely to be the most prominent for the cases of Veríssimo et al.[17] and Perpignan et al.[20], since leaner conditions had higher mass flows as fuel input was maintained. A more likely explanation is related to the alteration of prompt NO_x and the effect of *RR*, similarly to what is shown in Fig. 6. Due to the different mass flows and heat release characteristics, the amount and composition of recirculated gases is different for each Φ. Nonetheless, it is also important to take local phenomena into account, as changes in mixing patterns and heat losses have the potential to greatly influence the progress of chemistry.

4.0 CONCLUSIONS

The development of new combustion technologies aimed at reducing pollutant emissions is highly dependent on the capability of computational tools to predict emissions. The current paper examines the trends in NO_x emissions of an ITB intended to be operated under the FC regime. The analysis was performed by means of CRNs, and the effects of different chemical reaction mechanisms, reactants temperature, operating pressure, and recirculation ratio were shown.

https://doi.org/10.1017/aer.2019.12 Published online by Cambridge University Press

The conclusions of the analysis are summarized as follows:

1. The overall behaviour of NO_x emissions in systems with high recirculation ratios is complex and is dependent on several factors as reactants temperature, heat losses, amount of recirculation, and residence time.
2. The presence of combustion products and recirculation increase the relative importance of the prompt and NNH pathways, as well as NO reburning. The contribution of thermal NO_x tends to decrease with *RR*.
3. All investigated chemical reaction mechanisms resulted in overprediction of NO_x and in dominance of the prompt pathway. Prompt NO_x contribution was proportional to the overprediction, indicating that the reaction subset and its reaction rates for vitiated conditions may require revisions.
4. The role of prompt NO_x was shown to be prominent in the ITB experiments at atmospheric pressure and relatively low reactants temperature.
5. Increasing reactants' temperature did not alter the behaviour of NO_x with Φ. The overall emissions increased with increasing T_{in} and the NO_x peak moved to lower Φ due to lower residence times for higher temperatures.
6. The increase in operational pressure had complex effects on the behaviour of emissions with Φ. Leaner conditions had behaviour similar to that of conventional combustors (increase in NO_x). However, NO_x dropped with further increase in Φ due to the suppression of prompt NO_x production and due to the presence of reburning.
7. Given that all simulations herein presented were performed with CRNs, it is advisable to conduct experiments and simulations taking into account the fluid dynamics and turbulence effects in order to confirm the findings shown herein.

The consequences of the results discussed in this paper for the design of an ITB or any design intended to apply FC to aeronautical gas turbines are:

1. A successful ITB design should take advantage of the particularities of NO_x formation in lean conditions, optimizing emissions by altering residence times, operating pressure, and volume.
2. Classical correlations for the effect of pressure on the NO_x emissions of gas turbine combustors should not be employed for combustors with high recirculation rates.
3. The split of oxidiser between primary and dilution zones has more complex consequences in combustors with high recirculation than in conventional combustors. Besides influencing the amount of recirculation, the split also influences the chemistry of pollutant species.
4. The presence of extra degrees of freedom (energy split between primary and secondary combustors, and the design parameters of the ITB), as well as the existence of local minima in the pollutant emissions, makes the design of a dual-combustor system challenging but promising.

ACKNOWLEDGEMENTS

The authors would like to thank National Counsel of Technological and Scientific Development – Brazil (CNPq) for the financial support. The authors would also like to thank Prof. Yeshayhaou Levy from Technion (Israel Institute of Technology) for sharing the details of the experiments carried out within the AHEAD project.

https://doi.org/10.1017/aer.2019.12 Published online by Cambridge University Press

REFERENCES

1. MACINTOSH, A. and WALLACE, L. International aviation emissions to 2025: Can emissions be stabilised without restricting demand? *Energ Policy*, 2009, **37**, (1), pp 264–273.
2. ZHOU, W., WANG, T., YU, Y., CHEN, D. and ZHU, B. Scenario analysis of CO_2 emissions from China's civil aviation industry through 2030, *Appl Energy*, 2016, **175**, pp 100–108.
3. GLARBORG, P., MILLER, J.A., RUSCIC, B. and KLIPPENSTEIN, S.J. Modeling nitrogen chemistry in combustion, *Prog Energ Comb*, 2018, **67**, pp 31–68.
4. LEE, D.S., PITARI, G., GREWE, V., GIERENS, K., PENNER, J.E., PETZOLD, A., PRATHER, M.J., SCHUMANN, U., BAIS, A., BERNTSEN, T. and IACHETTI, D. Transport impacts on atmosphere and climate: Aviation, *Atmos Environ*, 2010, **44**, (37), pp 4678–4734.
5. PERPIGNAN, A.A.V., RAO, A.G. and ROEKAERTS, D.J.E.M. A review of flameless combustion and its potential towards gas turbines, *Prog Energ Comb*, 2018, **69**, pp 28–62.
6. YIN, F. and RAO, A.G. Performance analysis of an aero engine with interstage turbine burner, *Aeronaut J*, 2017, **121**, (1245), pp 1605–1626.
7. RAO, A.G., YIN, F. and VAN BUIJTENEN, J.P. A hybrid engine concept for multi-fuel blended wing body, *Aircraft Eng Aerospace Technol: An Int J*, 2014, **86**, (6), pp 483–493.
8. YIN, F. and RAO, A.G. Off-design performance of an interstage turbine burner turbofan engine, *J Eng Gas Turbine Power*, 2017, **139**, (8), pp 082603-1–082603-8.
9. LI, G., STANKOVIC, D., OVERMAN, N., CORNWELL, M., GUTMARK, E. and FUCHS, L. Experimental study of flameless combustion in gas turbine combustors, 44th AIAA Aerospace Sciences Meeting and Exhibit, 2006, Reno, Nevada, USA, p. 546.
10. NICOLLE, A. and DAGAUT, P. Occurrence of NO-reburning in MILD combustion evidenced via chemical kinetic modeling, *Fuel*, 2006, **85**, (17–18), pp 2469–2478.
11. WÜNNING, J.A. and WÜNNING, J.G. Flameless oxidation to reduce thermal NO-formation, *Prog Energ Comb*, 1997, **23**, pp 81–84.
12. MANCINI, M., SCHWÖPPE, P., WEBER, R. and ORSINO, S. On mathematical modelling of flameless combustion, *Combust Flame*, 2007, **150**, pp 54–59.
13. LI P., WANG. F., MI, J., DALLY, B.B., MEI, Z., ZHANG, J. and PARENTE, A. Mechanisms of NO formation in MILD combustion of CH_4/H_2 fuel blends, *Int J Hydrogen Energy* 2014, **39**, (33), 19187–19203.
14. CORREA, S.M. A review of NOx formation under gas-turbine combustion conditions, *Combust Sci Technol*, 1993, **87**, (1–6), pp 329–362.
15. LEFEBVRE, A.H. and BALLAL, D.R. *Gas Turbine Combustion: Alternative Fuels and Emissions*, CRC Press, 2010, Boca Raton, US.
16. RINK, K.K. and LEFEBVRE, A.H. Influence of fuel composition and spray characteristics on nitric oxide formation, ASME 1989 International Gas Turbine and Aeroengine Congress and Exposition, 1989, American Society of Mechanical Engineers, Toronto, Ontario, Canada.
17. VERÍSSIMO, A.S., ROCHA, A.M.A. and COSTA, M. Operational, combustion, and emission characteristics of a small-scale combustor, *Energ Fuel*, 2011, **25**, pp 2469–2480.
18. SORRENTINO, G., SABIA, P., DE JOANNON, M., BOZZA, P. and RAGUCCI, R. Influence of preheating and thermal power on cyclonic burner characteristics under mild combustion, *Fuel*, 2018, **233**, pp 207–214.
19. LEVY, Y., ERENBURG, V., SHERBAUM, V. and GAISSINSKI, I. Flameless oxidation combustor development for a sequential combustion hybrid turbofan engine. ASME Turbo Expo 2016: Turbomachinery Technical Conference and Exposition, 2016, American Society of Mechanical Engineers, Seoul, South Korea.
20. PERPIGNAN, A.A.V., TALBOOM, M.G., LEVY, Y. and RAO, A.G. Emission modeling of an interturbine burner based on flameless combustion, *Energy Fuels*, 2018, **32**, (1), pp 822–838.
21. LEBEDEV, A.B., SECUNDOV, A.M., STARIK, A.M., TITOVA, N.S. and SCHEPIN, A.M. Modeling study of gas-turbine combustor emission, *Proc Combust Inst*, 2009, **32**, pp 2941–2947.
22. LYRA, S. and CANT, R.S. Analysis of high pressure premixed flames using Equivalent Reactor Networks, *Fuel*, 2013, **107**, pp 261–268.
23. PARK, J., NGUYEN, T.H., JOUNG, D., HUH, K.Y. and LEE, M.C. Prediction of NOx and CO emissions from an industrial lean-premixed gas turbine combustor using a chemical reactor network model, *Energy Fuels*, 2013, **27**, pp 1643–1651.
24. CUOCI, A., FRASSOLDATI, A., STAGNI, A., FARAVELLI, T., RANZI, E. and BUZZI-FERRARIS, G. Numerical modeling of NOx formation in turbulent flames using a kinetic post-processing technique, *Energy Fuels*, 2013, **27**, pp 1104–1122.

https://doi.org/10.1017/aer.2019.12 Published online by Cambridge University Press

25. MONAGHAN, R.F.D., TAHIR, R., CUOCI, A., BOURQUE, G., FÜRI, M., GORDON, R.L., FARAVELLI, T., FRASSOLDATI, A. and CURRAN, H.J. Detailed multi-dimensional study of pollutant formation in a methane diffusion flame, *Energy Fuels*, 2012, **26**, pp 1598–1611.
26. FICHET, V., KANNICHE, M., PLION, P. and GICQUEL, O. A reactor network model for predicting NOx emissions in gas turbines, *Fuel*, 2010, **89**, pp 2202–2210.
27. GOODWIN, G., MOFFAT, H.K. and SPETH, R.L. Cantera: An object-oriented software toolkit for chemical kinetics, thermodynamics, and transport processes. Version 2.3.0. 2017, doi:10.5281/zenodo.170284. http://www.cantera.org
28. BOWMAN, C.T., HANSON, R.K., DAVIDSON, D.F., GARDINER, W.C., LISSIANSKI, V., SMITH, G.P., GOLDEN, D.M., FRENKLACH, M. and GOLDENBERG, M. http://www.me.berkeley.edu/gri_mech/
29. SMITH, G.P., GOLDEN, D.M., FRENKLACH, M., MORIARTY, N.W., EITENEER, B., GOLDENBERG, M., BOWMAN, C.T., HANSON, R.K., SONG, S., GARDINER, W.C., LISSIANSKI, V. and QIN Z. http://www.me.berkeley.edu/gri_mech/
30. KONNOV, A.A. Detailed reaction mechanism for small hydrocarbons combustion, Release 0.5, 2000.
31. PILLIER, L., DESGROUX, P., LEFORT, B., GASNOT, L., PAUWELS, J.F. and DA COSTA, I. NO prediction in natural gas flames using GDF-Kin® 3.0 mechanism NCN and HCN contribution to prompt-NO formation, *Fuel*, 2006, **85**, (7–8), pp 896–909.
32. RANZI, E., FRASSOLDATI, A., GRANA, R., CUOCI, A., FARAVELLI, T., KELLEY, A.P. and LAW, C.K. Hierarchical and comparative kinetic modeling of laminar flame speeds of hydrocarbon and oxygenated fuels. *Prog Energ Comb*, 2012, **38**, (4), pp 468–501.
33. KONNOV, A.A. Implementation of the NCN pathway of prompt-NO formation in the detailed reaction mechanism, *Combust Flame*, 2009, **156**, (11), pp 2093–2105.
34. GALLETTI, C., FERRAROTTI, M., PARENTE, A. and TOGNOTTI, L. Reduced NO formation models for CFD simulations of MILD combustion. *Int J Hydrogen Energy*, 2015, **40**, (14), pp 4884–4897.
35. BIAGIOLI, F. and GÜTHE, F. Effect of pressure and fuel–air unmixedness on NOx emissions from industrial gas turbine burners, *Combust Flame*, 2007, **151**, (1–2), pp 274–288.

APPENDIX

The table below shows the deactivated reaction for each chemical reaction mechanism employed for each reaction pathway. The overall guideline was to deactivate the least amount of reactions, prioritizing initiation reactions in order to impose less disturbance to the remainder of the mechanism. The error was estimated by summing the NO_x emissions obtained with each set of deactivated reactions and comparing the obtained value to that of the full mechanism.

Pathway	**Reactions**
	GRI 2.11
N_2O-Intermediate	$N_2O + OH \rightleftarrows N_2 + HO_2$ (184)
	$N_2O\ (+M) \rightleftarrows N_2 + O\ (+M)$ (185)
NNH	$NNH \rightleftarrows N_2 + H$ (204)
	$NNH\ (+M) \rightleftarrows N_2 + H\ (+M)$ (205)
	$NNH + O_2 \rightleftarrows HO_2 + N_2$ (206)
Prompt	$CH + N_2 \rightleftarrows HCN + N$ (240)
	$C + N_2 \rightleftarrows CN + N$ (239)
	$CH_2 + N_2 \rightleftarrows HCN + NH$ (242)
Reburning	$C + NO \rightleftarrows CN + O$ (244)
	$C + NO \rightleftarrows CO + N$ (245)
	$CH + NO \rightleftarrows HCN + O$ (246)
	$CH + NO \rightleftarrows H + NCO$ (247)
	$CH + NO \rightleftarrows HCO + N$ (248)

https://doi.org/10.1017/aer.2019.12 Published online by Cambridge University Press

	$CH_2 + NO \rightleftarrows H + HNCO$ (249)
	$CH_2 + NO \rightleftarrows HCN + OH$ (250)
	$CH_2 + NO \rightleftarrows H + HCNO$ (251)
	CH_2 (S) $+NO \rightleftarrows H + HNCO$ (252)
	CH_2 (S) $+NO \rightleftarrows HCN + OH$ (253)
	$CH_3 + NO \rightleftarrows H_2O + HCN$ (255)
	$HCCO + NO \rightleftarrows CO + HCNO$ (274)
	$HO_2 + NO \rightleftarrows NO_2 + OH$ (186)
	$HO_2 + NO \rightleftarrows O_2 + HNO$ (216)
	$H + NO\ (+M) \rightleftarrows HNO\ (+M)$ (212)
	$NO + O\ (+M) \rightleftarrows NO_2\ (+M)$ (187)
	$NO_2 + O \rightleftarrows NO + O_2$ (188)
Thermal	$N + NO \rightleftarrows N_2 + O$ (178)
	$N + O_2 \rightleftarrows NO + O$ (179)
	$N + OH \rightleftarrows NO + H$ (180)
	GRI 3.0
N_2O-Intermediate	$N_2O + OH \rightleftarrows N_2 + HO_2$ (257)
	$N_2O\ (+M) \rightleftarrows N_2 + O\ (+M)$ (258)
NNH	$NNH \rightleftarrows N_2 + H$ (280)
	$NNH\ (+M) \rightleftarrows N_2 + H\ (+M)$ (281)
	$NNH + O_2 \rightleftarrows HO_2 + N_2$ (283)
Prompt	$CH + N_2 \rightleftarrows HCN + N$ (322)
	$C + N_2 \rightleftarrows CN + N$ (321)
	$CH_2 + N_2 \rightleftarrows HCN + NH$ (327)
Reburning	$C + NO \rightleftarrows CN + O$ (329)
	$C + NO \rightleftarrows CO + N$ (330)
	$CH + NO \rightleftarrows HCN + O$ (331)
	$CH + NO \rightleftarrows H + NCO$ (332)
	$CH + NO \rightleftarrows HCO + N$ (333)
	$CH_2 + NO \rightleftarrows H + HNCO$ (334)
	$CH_2 + NO \rightleftarrows HCN + OH$ (335)
	$CH_2 + NO \rightleftarrows H + HCNO$ (336)
	CH_2 (S) $+NO \rightleftarrows H + HNCO$ (337)
	CH_2 (S) $+NO \rightleftarrows HCN + OH$ (338)
	CH_2 (S) $+NO \rightleftarrows H + HCNO$ (339)
	$CH_3 + NO \rightleftarrows H_2O + HCN$ (340)
	$CH_3 + NO \rightleftarrows H_2CN + OH$ (341)
	$HCCO + NO \rightleftarrows CO + HCNO$ (360)
	$HO_2 + NO \rightleftarrows NO_2 + OH$ (261)
	$HO_2 + NO \rightleftarrows O_2 + HNO$ (294)
	$H + NO\ (+M) \rightleftarrows HNO\ (+M)$ (289)
	$NO + O\ (+M) \rightleftarrows NO_2\ (+M)$ (262)
	$NO_2 + O \rightleftarrows NO + O_2$ (264)
Thermal	$N + NO \rightleftarrows N_2 + O$ (251)
	$N + O_2 \rightleftarrows NO + O$ (252)
	$N + OH \rightleftarrows NO + H$ (253)
	Konnov

https://doi.org/10.1017/aer.2019.12 Published online by Cambridge University Press

Pathway	**Reactions**
N_2O-Intermediate	N_2O (+M) $\rightleftarrows$ $N_2 + O$ (+M) (60)
	$N_2O + O \rightleftarrows N_2 + O_2$ (61)
	$N_2O + O \rightleftarrows NO + NO$ (62)
	$N_2O + H \rightleftarrows N_2 + OH$ (134)
	$N_2O + H \rightleftarrows NH + NO$ (135)
NNH	$NNH \rightleftarrows N_2 + H$ (102)
	NNH (+M) $\rightleftarrows$ $N_2 + H$ (+M) (103)
	$NNH + O_2 \rightleftarrows HO_2 + N_2$ (245)
	$NH + NH \rightleftarrows NNH + H$ (87)
	$NNH + H \rightleftarrows N_2 + H_2$ (104)
	$NNH + N \rightleftarrows N_2 + NH$ (105)
	$NNH + NH \rightleftarrows N_2 + NH_2$ (106)
	$NNH + NH_2 \rightleftarrows N_2 + NH_3$ (107)
	$NNH + NNH \rightleftarrows N_2H_2 + N_2$ (108)
	$N_2O + H \rightleftarrows NNH + O$ (136)
	$NNH + O \rightleftarrows N_2 + OH$ (243)
	$NNH + O \rightleftarrows NH + NO$ (222)
Prompt	$CH + N_2 \rightleftarrows NCN + H$ (1)
	$C + N_2 \rightleftarrows CN + N$ (1112)
	$N + N_2O \rightleftarrows NCN + NO$ (2)
	$NCN + H \rightleftarrows HCN + N$ (16)
	$NCN + O \rightleftarrows CN + NO$ (17)
	$NCN + OH \rightleftarrows HCN + NO$ (22)
	$NCN + OH \rightleftarrows HCN + NO$ (23)
	$NCN + O_2 \rightleftarrows NO + NCO$ (24)
	NH2 (+M) $\rightleftarrows$ NH + H (+M) (90)
	$NH + H_2 \rightleftarrows NH_2 + H$ (91)
	NH_3 (+M) $\rightleftarrows$ $NH_2 + H$ (+M) (98)
	$NH_3 + H \rightleftarrows NH_2 + H_2$ (100)
	$HNNO + H \rightleftarrows NH_2$+NO (143)
	$HNO + O_2 \rightleftarrows NO + HO2$ (169)
	$HNO + NH \rightleftarrows NH_2 + NO$ (172)
	$HNO + NH_2 \rightleftarrows NH3 + NO$ (173)
	$NH3 + O \rightleftarrows NH_2 + OH$ (194)
	$NH3 + OH \rightleftarrows NH_2 + H_2O$ (195)
	$NH_2 + HO_2 \rightleftarrows NH3 + O_2$ (197)
	$NH_2 + O \rightleftarrows HNO + H$ (199)
	$NH_2 + O \rightleftarrows NH + OH$ (200)
	$NH_2 + OH \rightleftarrows NH + H_2O$ (201)
	$NH_2 + HO_2 \rightleftarrows H_2NO + OH$ (204)
	$NH_2 + O_2 \rightleftarrows HNO + OH$ (205)
	$NH_2 + O_2 \rightleftarrows H_2NO + O$ (206)
	$NH_2 + NO \rightleftarrows NNH + OH$ (207)
	$NH_2 + NO \rightleftarrows N_2 + H_2O$ (208)
	$NH_2 + NO_2 \rightleftarrows N_2O + H_2O$ (210)
	$NH_2 + NO_2 \rightleftarrows H_2NO + NO$ (211)
	$NH + O_2 \rightleftarrows HNO + O$ (218)

https://doi.org/10.1017/aer.2019.12 Published online by Cambridge University Press

	$NH + O_2 \rightleftarrows NO + OH$ (219)
	$NH + NO \rightleftarrows N_2 + OH$ (223)
	$H_2NO + O_2 \rightleftarrows HNO + HO_2$ (259)
	$CH_2 + NO \rightleftarrows HCN + OH$ (1025)
	$HCN (+M) \rightleftarrows H + CN (+M)$ (1026)
	$C2 + N_2 \rightleftarrows CN + CN$ (1114)
	$H_2CN + O \rightleftarrows HCN + OH$ (1117)
	$CH + NO \rightleftarrows HCN + O$ (1127)
	CH_2 (S) $+NO \rightleftarrows HCN + OH$ (1139)
	$HCNO \rightleftarrows HCN + O$ (1140)
	$HCNO + H \rightleftarrows HCN + OH$ (1141)
	$HCNH + O \rightleftarrows HCN + OH$ (1158)
	$CN + H_2O \rightleftarrows HCN + OH$ (1162)
	$OH + HCN \rightleftarrows HOCN + H$ (1164)
	$OH + HCN \rightleftarrows HNCO + H$ (1165)
	$OH + HCN \rightleftarrows NH_2 + CO$ (1166)
	$HCN + O \rightleftarrows NCO + H$ (1168)
	$HCN + O \rightleftarrows NH + CO$ (1169)
	$HCN + O \rightleftarrows CN + OH$ (1170)
	$CN + H_2 \rightleftarrows HCN + H$ (1171)
	$CN + O_2 \rightleftarrows NCO + O$ (1173)
	$HNCO + H \rightleftarrows H_2 + NCO$ (1181)
	$HNCO + H \rightleftarrows NH_2 + CO$ (1182)
	$HNCO + O \rightleftarrows NCO + OH$ (1184)
	$HNCO + O \rightleftarrows NH + CO_2$ (1185)
	$HNCO + O \rightleftarrows HNO + CO$ (1186)
	$HNCO + OH \rightleftarrows NCO + H_2O$ (1187)
	$HNCO + OH \rightleftarrows NH_2 + CO_2$ (1188)
	$NCO + H \rightleftarrows NH + CO$ (1193)
	$NCO + O \rightleftarrows NO + CO$ (1194)
	$NCO + NO \rightleftarrows N_2O + CO$ (1199)
	$NCO + NO \rightleftarrows N_2 + CO_2$ (1200)
	$NCO + O_2 \rightleftarrows NO + CO_2$ (1201)
Reburning	$C + NO \rightleftarrows CN + O$ (1126)
	$C + NO \rightleftarrows CO + N$ (1218)
	$CH + NO \rightleftarrows HCN + O$ (1127)
	$CH + NO \rightleftarrows H + NCO$ (1130)
	$CH_2 + NO \rightleftarrows H + HNCO$ (1131)
	$CH_2 + NO \rightleftarrows HCN + OH$ (1025)
	$CH_2 + NO \rightleftarrows H + HCNO$ (1132)
	CH_2 (S) $+NO \rightleftarrows HCN + OH$ (1139)
	$CH_3 + NO \rightleftarrows H_2O + HCN$ (1135)
	$HCCO + NO \rightleftarrows CO + HCNO$ (1137)
	$HO_2 + NO \rightleftarrows NO_2 + OH$ (153)
	$HO_2 + NO \rightleftarrows O_2 + HNO$ (169)
	$H + NO\ (+M) \rightleftarrows HNO\ (+M)$ (164)
	$NO + O\ (+M) \rightleftarrows NO_2\ (+M)$ (65)
	$NO_2 + O \rightleftarrows NO + O_2$ (67)

https://doi.org/10.1017/aer.2019.12 Published online by Cambridge University Press

Pathway	**Reactions**
Thermal	$N + NO \rightleftarrows N_2 + O$ (56)
	$N + O_2 \rightleftarrows NO + O$ (57)
	$N + OH \rightleftarrows NO + H$ (133)
	GDF-Kin® 3.0
N_2O-Intermediate	$N_2O + OH \rightleftarrows N_2 + HO_2$ (776)
	$N_2O\ (+M) \rightleftarrows N_2 + O\ (+M)$ (778)
NNH	$NNH + H \rightleftarrows N_2 + H_2$ (740)
	$NNH\ (+M) \rightleftarrows N_2 + H\ (+M)$ (738)
	$NNH + OH \rightleftarrows N_2 + H_2O$ (741)
	$NNH + O \rightleftarrows N_2O + H$ (744)
Prompt	$CH + N_2 \rightleftarrows NCN + H$ (868)
	$C + N_2 \rightleftarrows CN + N$ (826)
	$CH_2 + N_2 \rightleftarrows HCN + NH$ (867)
Reburning	$C + NO \rightleftarrows CN + O$ (783)
	$CN + NO \rightleftarrows NCO + N$ (819)
	$CH + NO \rightleftarrows HCN + O$ (784)
	$CH_2 + NO \rightleftarrows HCN + OH$ (787)
	$CH_2 + NO \rightleftarrows H + HCNO$ (786)
	$CH_2\ (S) + NO \rightleftarrows HCN + OH$ (785)
	$CH_3 + NO \rightleftarrows H_2O + HCN$ (788)
	$HCCO + NO \rightleftarrows CO + HCNO$ (790)
	$HO_2 + NO \rightleftarrows NO_2 + OH$ (762)
	$HO_2 + NO \rightleftarrows O_2 + HNO$ (751)
	$H + NO\ (+M) \rightleftarrows HNO\ (+M)$ (764)
	$NO + O\ (+M) \rightleftarrows NO_2\ (+M)$ (769)
	$NO_2 + O \rightleftarrows NO + O_2$ (768)
Thermal	$N + NO \rightleftarrows N_2 + O$ (699)
	$N + O_2 \rightleftarrows NO + O$ (702)
	$N + OH \rightleftarrows NO + H$ (703)
	POLIMI C1C3HT
N_2O-Intermediate	$N_2O + OH \rightleftarrows N_2 + HO_2$ (815)
	$N_2O\ (+M) \rightleftarrows N_2 + O\ (+M)$ (809)
NNH	$NNH \rightleftarrows N_2 + H$ (643)
	$NNH + O_2 \rightleftarrows HO_2 + N_2$ (648)
Prompt	$CH + N_2 \rightleftarrows HCN + N$ (769)
	$C + N_2 \rightleftarrows CN + N$ (771)
	$CH_2 + N_2 \rightleftarrows HCN + NH$ (767)
Reburning	$C + NO \rightleftarrows CN + O$ (772)
	$C + NO \rightleftarrows CO + N$ (773)
	$CH + NO \rightleftarrows HCN + O$ (774)
	$CH + NO \rightleftarrows H + NCO$ (775)
	$CH + NO \rightleftarrows HCO + N$ (776)
	$CH_2 + NO \rightleftarrows H + HNCO$ (781)
	$CH_2 + NO \rightleftarrows HCN + OH$ (779)
	$CH_2 + NO \rightleftarrows H + HCNO$ (783)
	$CH_2\ (S) + NO \rightleftarrows H + HNCO$ (782)

https://doi.org/10.1017/aer.2019.12 Published online by Cambridge University Press

	CH_2 (S) $+NO \rightleftarrows HCN + OH$ (780)
	$CH_3 + NO \rightleftarrows H_2O + HCN$ (764)
	$HCCO + NO \rightleftarrows CO + HCNO$ (805)
	$HO_2 + NO \rightleftarrows NO_2 + OH$ (665)
	$HO_2 + NO \rightleftarrows O_2 + HNO$ (673)
	$H + NO\ (+M) \rightleftarrows HNO\ (+M)$ (669)
	$NO + O\ (+M) \rightleftarrows NO_2\ (+M)$ (666)
	$NO_2 + O \rightleftarrows NO + O_2$ (701)
Thermal	$N + NO \rightleftarrows N_2 + O$ (623)
	$N + O_2 \rightleftarrows NO + O$ (622)
	$N + OH \rightleftarrows NO + H$ (621)

https://doi.org/10.1017/aer.2019.12 Published online by Cambridge University Press